7016 *Inorg. Chem.* **2010**, *49*, 7016–7027
DOI: 10.1021/ic100609h

Inorganic Chemistry
Article

Hydrogen and Copper Ion Induced Molecular Reorganizations in Two New Scorpiand-Like Ligands Appended with Pyridine Rings

Salvador Blasco,[†] Begoña Verdejo,[†] M. Paz Clares,[†] Carmen E. Castillo,[‡] Andrés G. Algarra,[‡] Julio Latorre,[§] M. Angeles Máñez,[‡] Manuel G. Basallote,*[,‡] Conxa Soriano,[∥] and Enrique García-España*[,†]

[†]*Departamento de Química, Inorgánica, Universidad de Valencia, Instituto de Ciencia Molecular, Edificio de Institutos de Paterna Apdo 22085, 46071, Valencia, Spain,* [‡]*Departamento de Ciencia de los Materiales e Ingeniería Metalúrgica, Facultad de Ciencias, Universidad de Cádiz, Apdo 40, Puerto Real, 11510 Cádiz, Spain,* [§]*Departamento de Química Inorgánica, Universidad de Valencia, Instituto de Ciencia de Materiales, C/Dr. Moliner 50, 46100 Burjasot, Valencia, Spain, and* [∥]*Departamento de Química Orgánica, Universidad de Valencia, Instituto de Ciencia Molecular, Edificio de Institutos de Paterna Apdo 22085, 46071, Valencia, Spain*

Received March 31, 2010

The synthesis of two new ligands constituted of a tris(2-aminoethyl)amine moiety linked to the 2,6 positions of a pyridine spacer through methylene groups in which the hanging arm is further functionalized with a 2-pycolyl (**L1**) or 3-pycolyl (**L2**) group is presented. The protonation of **L1** and **L2** and formation of Cu^{2+} complexes have been studied using potentiometric, NMR, X-ray, and kinetic experiments. The results provide new information about the relevance of molecular movements in the chemistry of this kind of so-called scorpiand ligand. The comparison between these two ligands that only differ in the position of the substituent at the arm reveals important differences in both thermodynamic and kinetic properties. The Cu^{2+} complex with **L1** is several orders of magnitude more stable than that with **L2**, surely because in the latter case the pyridine nitrogen at the pendant arm is unable to coordinate to the metal ion with the ligand acting as hexadentate, a possibility that occurs in the case of $[Cu\mathbf{L1}]^{2+}$, as demonstrated by its crystal structure. Significant differences are also found between both ligands in the kinetic studies of complex formation and decomposition. For **L1**, those processes occur in a single kinetic step, whereas for **L2** they occur with the formation of a detectable reaction intermediate whose structure corresponds to that resulting from the movement typical of scorpiands. Another interesting conclusion derived from kinetic studies on complex formation is that the reactive form of the ligand is H_3L^{3+} for **L1** and H_2L^{2+} for **L2**. DFT calculations are also reported, and they allow a rationalization of the kinetic results relative to the reactive forms of the ligands in the process of complex formation. In addition, they provide a full picture of the mechanistic pathway leading to the formation of the first Cu−N bond, including outer-sphere complexation, water dissociation, and reorganization of the outer-sphere complex.

Introduction

Organized molecular motions are at the heart of crucial biological processes such as protein folding, transmission of nerve impulses, etc.[1] In recent years, these motions have inspired the research of a number of groups that have prepared more or less structurally sophisticated molecules able to perform movements and/or reorganizations controlled by

*To whom correspondence should be addressed. Tel.: (+34) 956-016-339 (M.G.B.). Fax: (+34) 956-016−288 (M.G.B.). E-mail: manuel.basallote@uca.es (M.G.B.); enrique.garcia-es@uv.es (E.G.-E.).

(1) (a) Yoshida, M.; Muneyuki, E.; Hisabori, T. *Nat. Rev. Mol. Cell. Biol.* **2001**, *2*, 669–677. (b) Boyer, P. D. *Nature* **1999**, *402*, 247–249. (c) Stock, D.; Leslie, A. G. W.; Walker, J. E. *Science* **1999**, *286*, 1700–1705. (d) Namba, K.; Vonderviszt, F. Q. *Q. Rev. Biophys.* **1997**, *30*, 1–65. (e) Berg, H. C. *Annu. Rev. Biochem.* **2003**, *72*, 19–54. (f) Colbran, R. J. *Biochem. J.* **2004**, *378*, 1–16. (g) Saibil, H. R.; Ranson, N. A. *Trends. Biochem. Sci.* **2002**, *27*, 627–632. (h) Braig, K.; Otwinowski, Z.; Hedge, R.; Boisvert, D. C.; Joachimiak, A.; Horwich, A. L.; Sigler, P. B. *Nature* **1994**, *371*, 578–586. (i) Wang, J.; Boisvert, D. C. *J. Mol. Biol.* **2003**, *327*, 843–855. (j) Rossmann, M. G; Mesyanzhinov, V. V.; Arisaka, F.; Leiman, P. G. *Curr. Opin. Struct. Biol.* **2004**, *14*, 171–180.

(2) (a) Raehm, L.; Sauvage, J.-P. *Struct. Bonding* (*Berlin*) **2001**, *99*, 55–78. (b) Pease, A. R.; Jeppesen, J. O.; Stoddart, J. F.; Luo, Y.; Collier, C. P.; Heath, J. R. *Acc. Chem. Res.* **2001**, *34*, 433–444. (c) Ballardini, R.; Balzani, V.; Credi, A.; Gandolfi, M. T.; Venturi, M. *Acc. Chem. Res.* **2001**, *34*, 445–455. (d) Amendola, V.; Fabbrizzi, L.; Mangano, C.; Pallavicini, P. *Acc. Chem. Res.* **2001**, *34*, 488–493. (e) Feringa, B. L. *Acc. Chem. Res.* **2001**, *34*, 504–513. (f) Balzani, V.; Credi, A.; Venturi, M. *Chem. Soc. Rev.* **2009**, *38*, 1542–1550. (g) Kinbara, K.; Aida, T., *Chem. Rev.* **2005**, *105*, 1377−1400. For a book dealing with this topic see: *Intelligent Materials*; Shahinpoor, M., Schneider, H.-J., Eds.; RSC Publishing: Cambridge, U. K., 2008.

(3) (a) Dietrich-Buchecker, C. O.; Sauvage, J. -P.; Kintzinger, J. P. *Tetrahedron Lett.* **1983**, *24*, 5095–5098. (b) Bisell, R. A.; Cordova, E.; Kaifer, A. E.; Stoddart, J. F. *Nature* **1994**, *369*, 133–137. (c) Cesario, M.; Dietrich-Buchecker, C. O.; Guilhem, J.; Pascard, C.; Sauvage, J. P. *J. Chem. Soc., Chem. Commun.* **1985**, 244–247. (d) Collin, J. -P.; Heitz, V.; Sauvage, J. -P. *Top. Curr. Chem.* **2005**, *262*, 29–62. (e) Balzani, V.; Credi, A.; Venturi, M. *Molecular Devices and Machines - A Journey into the Nanoworld*; WILEY-VCH: Weinheim, Germany, 2003.

Published on Web 07/08/2010

external stimuli that can be of a chemical (pH gradients, presence of a metal ion, etc) or a physical nature (light irradiation, flux of electrons, etc).[2] The preparation of the first catenanes and rotaxanes, in which a molecule is either interlocked or threaded with respect to another one, represented a real breakthrough in this field of chemistry.[3] Another strategy for achieving systems able to perform controlled molecular motions consists of making molecules having a rigid and a flexible unit, so that the latter unit can change its position with respect to the former one responding to a given chemical or physical impulse. Within this topic, Kaden and Lotz in Basel and Fabbrizzi's group in Pavia started several years ago to prepare polyamines consisting of a fixed macrocyclic core appended with a flexible arm, giving great impetus to this topic.[4,5] Since then, this field of chemistry has remarkably expanded, and the discovery of many new compounds has increased the size of the polyaza scorpiand family.[6]

Recently, we described a couple of new ligands belonging to this category.[7] These ligands were built up linking a tris-(2-aminoethyl)amine unit to the 2,6 positions of a pyridine spacer through methylene groups (**L3**), further functionalizing the hanging arm with a 1-methylnaphthyl unit (**L4**; see Chart 1). We showed that in the case of **L4**, the folding movement of the arm toward the macrocyclic core could be achieved not only by the coordination of Cu^{2+} but also by the formation of internal hydrogen bonds in the mono- and diprotonated forms of **L4**. Triprotonation of **L4** produces the breaking of the hydrogen bond network and the displacement of the hanging arm far apart from the macrocyclic core in order to minimize electrostatic repulsions between the charged ammonium groups.

Here, we present the preparation of two **L3** derivatives in which the primary amino group of the tails has been functionalized with 2-pycolyl or 3-pycolyl groups (compounds **L1** and **L2** in Chart 1). **L1** has in its tail a potential double anchoring moiety so that the encapsulated metal ions can reach hexa-coordination by nitrogen atoms and can, therefore, display distinct thermodynamics and kinetics of formation from the related compounds **L3** and **L4**. In contrast, the disposition of the pyridinic nitrogen in **L2** hinders its coordination simultaneously with the other donors, so that hexacoordination appears unlikely. We report here the protonation behavior of the ligands, the formation of Cu^{2+} complexes, and their dissociation and formation kinetics, paying a particular attention to an analysis of the influence of

Chart 1

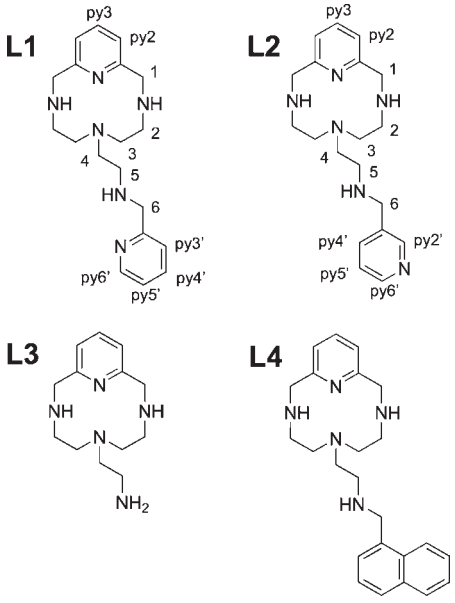

the substitution of the pyridine rings on the acid−base and coordination behaviors. Significant thermodynamic and kinetic differences are found between both systems. DFT calculations have allowed the rationalization of the kinetic results, providing a full picture of the mechanistic pathway leading to complex formation from aquated Cu^{2+} and protonated ligands. When compared with the previously reported **L3** and **L4** ligands, the Cu^{2+} complexes with **L1** and **L2** also show significant differences; whereas the chemistry of the Cu^{2+}−**L1** system is dominated by a very stable hexacoordinate complex not possible for **L3** and **L4**, the chemistry of Cu^{2+}−**L2** resembles more that of the **L3** and **L4** complexes, although the presence of an additional pyridinic nitrogen in the side chain allows for a faster initiation of the complex formation process.

Experimental Section

The synthesis of the ligands has been carried out following the general procedure described for the preparation of **L4**,[7] which consists of the reaction of 6-(2-aminoethyl)-3,6,9-triaza-1(2,6)-pyridinacyclodecaphane (**L3**) and the corresponding pyridine carbaldehyde in ethanol followed by reduction with sodium borohydride.

Synthesis. 6-[2-(N-Methyl-2-pyridyl)ethylamino]-3,6,9-triaza-1(2,6)-pyridinacyclodecaphane Hydrochloride (L1·3HCl). 6-(2-Aminoethyl)- 3,6,9-triaza-1(2,6)-pyridinacyclodecaphane (0.58 g, 2.33 mmol) and pyridine-2-carbaldehyde (0.32 g, 2.96 mmol) are dissolved in 100 mL of dry ethanol and stirred at room temperature for 2 h. Then, sodium borohydride (1.3 g, 34 mmol) is added, and the bulk is stirred for 2 h more. Then, the solution is vacuum evaporated and extracted with $CHCl_3/H_2O$ (6 × 100). The organic phase is taken to dryness and redissolved in dry ethanol. The hydrochloride salt of the product is precipitated by adding a concentrated hydrochloride acid solution. ^{1}H NMR (D_2O, 300 MHz): δ_H 2.93 (t, J = 5 Hz, 4H), 3.13 (t, J = 8 Hz, 2H), 3.28 (t, J = 5 Hz, 4H), 3.45 (t, J = 8 Hz, 2H), 4.57 (s, 2H), 4.64 (s, 4H), 7.45 (d, J = 8 Hz, 2H), 7.75 (ddd, $J_1 = J_2$ = 8 Hz, J_3 = 1 Hz, 1H), 7.83 (d, J = 8 Hz, 1H), 7.96 (t, J = 8 Hz, 1H), 8.25 (ddd, $J_1 = J_2$ = 8 Hz, J_3 = 2 Hz, 1H), 8.72(dd, J_1 = 5 Hz, J_2 = 1 Hz, 1H). ^{13}C NMR (D_2O, 75.43 MHz): δ_C 43.9, 46.2, 49.8, 50.0, 50.8, 51.2, 122.5, 126.5, 126.6, 140.1, 143.3, 146.8, 147.6, 149.2. Anal. Calcd. for $C_{19}H_{28}N_6 \cdot 3HCl$: C, 50.68; H, 6.94; N, 18.75. Found: C, 50.3, H, 7.1; N 18.5.

6-[2-(N-Methyl-3-pyridyl)ethylamino]-3,6,9-triaza-1(2,6)-pyridinacyclodecaphane Hydrochloride (L2·3HCl). The same procedure

(4) Lotz, T. J.; Kaden, T. A. *J. Chem. Soc., Chem. Commun.* **1977**, 15–16.
(5) Pallavicini, P. S.; Perotti, A.; Poggi, A.; Seghi, B.; Fabbrizzi, L. *J. Am. Chem. Soc.* **1987**, *109*, 5139–5144.
(6) (a) Soibinet, M.; Gusmeroli, D.; Siegfried, L.; Kaden, T. A.; Palivan, C.; Schweiger, A. J. *Dalton Trans.* **2005**, 2138–2146. (b) Siegfried, L.; Kaden, T. A. *Dalton Trans.* **2005**, 1136–1140. (c) Siegfried, L.; Kaden, T. A. *J. Chem. Soc., Dalton Trans.* **2005**, 3079–3082. (d) Amendola, V.; Fabbrizzi, L; Licchelli, M.; Mangano, C.; Pallavicini, P.; Parodi, L; Poggi, A. *Coord. Chem. Rev.* **1999**, *192*, 649–669. (e) Fabbrizzi, L.; Foti, F.; Licchelli, M.; Poggi, A.; Taglieti, A; Vazquez, M. *Adv. Inorg. Chem.* **2007**, *59*, 81–107. (f) Herrera, A. M.; Staples, R. J.; Kryatov, S. V.; Nazarenko, A. Y.; Rybak-Akimova, E. V. *Dalton Trans.* **2003**, 846–856. (g) Organo, V. G.; Filatov, A. S.; Quartararo, J. S.; Friedman, Z. M.; Rybak-Akimova, E. *Inorg. Chem.* **2009**, *48*, 8456–8468. (h) Bencini, A.; Bianchi, A.; Lodeiro, C.; Masotti, A.; Parola, A. J.; Pina, F.; Seixas de Melo, J.; Valtancoli, B *Chem. Commun.* **2000**, 1639–1640. (i) Bencini, A.; Berni, E.; Bianchi, A.; Fornasari, P.; Giorgi, C.; Lima, J. C.; Lodeiro, C.; Melo, M. J.; de Melo, J. S.; Parola, A. J.; Pina, F.; Pina, J.; Valtancoli, B. *Dalton Trans.* **2004**, 2180–2187.
(7) Verdejo, B.; Ferrer, A.; Blasco, S.; Castillo, C. E.; Gonzalez, J.; Latorre, J.; Mañez, M. A.; Basallote, M. G.; Soriano, C.; Garcia-España, E. *Inorg. Chem.* **2007**, *46*, 5707–5719.

applies for the synthesis of **L1**, but pyridine-3-carbaldehyde is used instead of pyridine-2-carbaldehyde. ^{1}H NMR (D_2O, 300 MHz): δ_H 2.94 (t, J = 5 Hz, 4H), 3.11 (t, J = 7 Hz, 2H), 3.30 (t, J = 5 Hz, 4H), 3,48 (t, J = 7 Hz, 2H), 4.64 (s, 4H), 4.62 (s, 2H), 7.45 (d, J = 8 Hz, 2H), 7.96 (t, J = 8 Hz, 1H), 8.20 (dd, J_1 = 8 Hz, J_2 = 6 Hz, 1H), 8.83 (d, J = 8 Hz, 1H), 8.91 (d, J = 6 Hz, 1H), 9.05 (d, J = 2 Hz, 1H). ^{13}C NMR (D_2O, 75.43 MHz): δ_C 43.9, 45.8, 47.7, 49.5, 50.4, 50.8, 122.1, 128.0, 131.1, 142.5, 148.7, 148.8. Anal. Calcd. for $C_{19}H_{28}N_6 \cdot 3HCl$: C, 50.68; H, 6.94; N, 18.75. Found: C, 50.8, H, 7.0; N 18.8.

[CuL1](ClO$_4$)$_2$. To an aqueous solution (5 mL) of **L1**·3HCl (0.017 g, 0.038 mmol) was added $Cu(ClO_4)_2 \cdot 6H_2O$ (0.011 g, 0.03 mmol) in water (5 mL) dropwise with stirring. The pH of the solution was adjusted to 7 by the addition of 0.5 M NaOH. After the mixture was stirred for 2 h at room temperature, it was filtered. Blue crystals were obtained in 50% yield by slow evaporation of the solvent. Anal. Calcd. for $C_{19}H_{28}N_6Cl_2O_8Cu$: C, 37.73; H, 4.66; N, 13.88. Found: C, 37.5, H, 4.7; N 13.5. ***Caution!*** *Perchlorate salts of compounds containing organic ligands are potentially explosive and should be handled with care.*

Crystallographic Analysis. An analysis of single crystals of [Cu**L1**](ClO$_4$)$_2$ was carried out with an Enraf-Nonius KAPPA CCD single-crystal diffractometer (λ = 0.71073 Å). The structure was solved using the program SHELXS-86.[8] Structural refinement was performed by means of the program SHELXL-97.[9] Molecular plots were produced with either the program MERCURY[10] or ORTEP.[11] Crystal data, data collection parameters, and results of the analysis are listed in Table S1, Supporting Information.

EMF Measurements. The potentiometric titrations were carried out at 298.1 ± 0.1 K using 0.15 M $NaClO_4$ as the supporting electrolyte. The experimental procedure (buret, potentiometer, cell, stirrer, microcomputer, etc.) has been fully described elsewhere.[12] The acquisition of the EMF data was performed with the computer program PASAT.[13] The reference electrode was a Ag/AgCl electrode in saturated KCl solution. The glass electrode was calibrated as a hydrogen-ion concentration probe by the titration of previously standardized amounts of HCl with CO_2-free NaOH solutions and the equivalent point determined by the Gran's method,[14,15] which gives the standard potential, $E^{\circ\prime}$, and the ionic product of water (pK_w = 13.73(1)).

The computer program HYPERQUAD[16] was used to calculate the protonation and stability constants. The pH range investigated was 2.5−11.0, and the concentration of the metal ion and of the ligands ranged from 1×10^{-3} to 5×10^{-3} mol·dm^{-3} with M/L molar ratios varying from 2:1 to 1:2. The different titration curves for each system (at least two with over 50 experimental data points) were treated either as a single set or as separated curves without significant variations in the values of the stability constants. Finally, the sets of data were merged together and treated simultaneously to give the final stability constants. In the case of the system Cu^{2+}−**L1**, the high stability of the Cu**L1**$^{2+}$ complex formed prevented a significant enough competition with the protonation processes. For a 1:1 molar ratio with [Cu^{2+}] = [**L1**] = 1×10^{-3} M, 92% of the complex was already formed at pH = 3 and 99% at pH = 3.5 (see distribution diagram in the Supporting Information). Therefore, to check the value obtained from the direct titrations, a competition titration with **L3** was also used. Namely, solutions containing Cu^{2+}, **L1**, and **L3** in equimolar amounts were titrated with a base. The constants previously determined for the system Cu^{2+}−**L3** were taken as known parameters and those of the system Cu^{2+}−**L1** fitted with the HYPERQUAD program.[16]

Kinetic Experiments. The kinetic experiments were carried out at 298.1 ± 0.1 K with either a Cary 50-BIO spectrophotometer or an Applied Photophysics SX17MV stopped-flow instrument provided with a PDA-1 diode array detector. The ionic strength was adjusted to 0.15 M for formation studies and 1.0 M for decomposition studies by adding the required amount of $NaClO_4$. The kinetic work on complex decomposition were carried out under pseudo-first-order conditions of acid excess, and the solutions contained Cu^{2+} and the corresponding ligand in a 1:1 molar ratio. The pH was adjusted with NaOH to values at which the fomation of the CuL^{2+} complexes in solution is maximized. The kinetic experiments provided spectral changes with time that were analyzed with the SPECFIT program.[17] For kinetic studies on complex formation, a solution of the ligand whose pH had been previously adjusted with $HClO_4$ and NaOH was mixed in the stopped-flow instrument with a solution of the same pH and containing the same concentration of Cu^{2+}.

Theoretical Calculations. Calculations were carried out with the Gaussian 03 package[18] and the unrestricted Becke three-parameter hybrid functional combined with Lee−Yang−Parr correlation functional (UB3LYP).[18,19] The double-ξ pseudo-orbital basis set LanL2DZ was employed for the copper atom,[20] while the D95 V basis set, augmented by a set of standard p and d polarization fuctions (D95Vp) was used for all other atoms.[21] Optimizations were performed initially in the gas phase, and subsequent reoptimizations were carried out in solution (water solvent, ε = 78.39) by employing the CPCM method.[22] Efforts were made to find the lowest energy conformation by comparing the structures optimized from different starting geometries. Harmonic frequency calculations were performed to confirm

(8) Sheldrick, G. M.; Kruger, C.; Goddard, R. *Crystallographic Computing*; Clarendon Press: Oxford, England, 1985; p 1175.
(9) Sheldrick, G. M. *Acta Crystallogr., Sect. A* **2008**, *64*, 112–122.
(10) Macrae, C. F.; Edgington, P. R.; McCabe, P.; Pidcock, E.; Shields, G. P.; Taylor, R.; Towler, M.; Streek, J. V. D. *J. Appl. Crystallogr.* **2006**, *39*, 453–457.
(11) Johnson, C. K. *ORTEP*, Report ORNL-3794; Oak Ridge National Laboratory: Oak Ridge, TN, 1971.
(12) García-España, E.; Ballester, M.-J.; Lloret, F.; Moratal, J. M.; Faus, J.; Bianchi, A. *J. Chem. Soc., Dalton Trans.* **1988**, 101–104.
(13) Fontanelli, M.; Micheloni, M. Program for the automatic control of the microburette and the acquisition of the electromotive force readings. *Proceedings of the I Spanish-Italian Congress on Thermodinamics of Metal Complexes*; Diputación de Castellón: Castellón, Spain, 1990.
(14) Gran, G. *Analyst* **1952**, *77*, 661–671.
(15) Rossotti, F. J.; Rossotti, H. *J. Chem. Educ.* **1965**, *42*, 375–378.
(16) Gans, P.; Sabatini, A.; Vacca, A. *Talanta* **1996**, *43*, 1739–1753.
(17) (a) *SPECFIT, A Program for Global Least Square Fitting of Equilibrium and Kinetic Systems using Factor Analysis and Marquardt Minimization*, version 1−26, 24; Spectrum Software Associates: Chapel Hill, NC, 1996. (b) Gampp, H.; Maeder, M.; Meyer, C. J.; Zuberbuhler, A. D. *Talanta* **1985**, *32*, 95–101. (c) Gampp, H.; Maeder, M.; Meyer, C. J.; Zuberbuhler, A. D. *Talanta* **1985**, *32*, 257–264. (d) Gampp, H.; Maeder, M.; Meyer, C. J.; Zuberbuhler, A. D. *Talanta* **1986**, *33*, 943–951.
(18) Frisch, M. J.; Trucks, G. W.; Schlegel, H. B.; Scuseria, G. E.; Robb, M. A.; Cheeseman, J. R.; Montgomery, J. A., Jr.; Vreven, T.; Kudin, K. N.; Burant, J. C.; Millam, J. M.; Iyengar, S. S.; Tomasi, J.; Barone, V.; Mennucci, B.; Cossi, M.; Scalmani, G.; Rega, N.; Petersson, G. A.; Nakatsuji, H.; Hada, M.; Ehara, M.; Toyota, K.; Fukuda, R.; Hasegawa, J.; Ishida, M.; Nakajima, T.; Honda, Y.; Kitao, O.; Nakai, H.; Klene, M.; Li, X.; Knox, J. E.; Hratchian, H. P.; Cross, J. B.; Bakken, V.; Adamo, C.; Jaramillo, J.; Gomperts, R.; Stratmann, R. E.; Yazyev, O.; Austin, A. J.; Cammi, R.; Pomelli, C.; Ochterski, J. W.; Ayala, P. Y.; Morokuma, K.; Voth, G. A.; Salvador, P.; Dannenberg, J. J.; Zakrzewski, V. G.; Dapprich, S.; Daniels, A. D.; Strain, M. C.; Farkas, O.; Malick, D. K.; Rabuck, A. D.; Raghavachari, K.; Foresman, J. B.; Ortiz, J. V.; Cui, Q.; Baboul, A. G.; Clifford, S.; Cioslowski, J.; Stefanov, B. B.; Liu, G.; Liashenko, A.; Piskorz, P.; Komaromi, I.; Martin, R. L.; Fox, D. J.; Keith, T.; Al-Laham, M. A.; Peng, C. Y.; Nanayakkara, A.; Challacombe, M.; Gill, P. M. W.; Johnson, B.; Chen, W.; Wong, M. W.; Gonzalez, C.; Pople, J. A. *Gaussian 03*, Revision E.01; Gaussian, Inc.: Wallingford, CT, 2004.
(19) (a) Becke, A. D. *J. Chem. Phys.* **1993**, *98*, 5648–5652. (b) Lee, C. T.; Yang, W. T.; Parr, R. G. *Phys. Rev. B* **1988**, *37*, 785–789.
(20) (a) Hay, P. J.; Wadt, W. R. *J. Chem. Phys.* **1985**, *82*, 270–283. (b) Wadt, W. R.; Hay, P. J. *J. Chem. Phys.* **1985**, *82*, 284–298. (c) Hay, P. J.; Wadt, W. R. *J. Chem. Phys.* **1985**, *82*, 299–310.
(21) Huzinaga, S.; Andzelm, J.; Klobukowski, M.; Radzio-Andzelm, E.; Sakai, Y.; Tatewaki, H. *Gaussian basis sets for molecular calculations*; Elsevier: Amsterdam, 1984.
(22) Cossi, M.; Rega, N.; Calmani, G.; Barone, V. *J. Comput. Chem.* **2003**, *24*, 669–681.

Table 1. Stepwise Protonation Constants for **L1** and **L2** Determined at 298.1 K in 0.15 M $NaClO_4$[a]

reaction[b]	L1	L2	L3	L4
$H + L \leftrightarrows HL$	10.21(1)[c]	9.84(5)	10.20(6)	10.01(1)
$H + HL \leftrightarrows H_2L$	8.84(1)	8.52(8)	9.18(3)	8.71(1)
$H + H_2L \leftrightarrows H_3L$	7.39(2)	6.8(1)	7.84(4)	7.26(1)
$H + H_3L \leftrightarrows H_4L$	3.12(2)	3.4(1)		

[a] The corresponding ones for **L3** and **L4** taken from ref 7 are also included. [b] Charges omitted. [c] Values in parentheses are standard deviations in the last significant figure.

that the calculated structures were minima. Due to problems caused by the large number of vertices in the cavity surface during the scan calculations, the OFAC = 0.7 and Rmin = 0.5 options were employed throughout these optimizations.

Results and Discussion

Acid−Base Behavior of L1 and L2. Table 1 collects the stepwise protonation constants of **L1** and **L2** determined in 0.15 M $NaClO_4$ at 298.1 K along with those we have previously reported for the parent compound **L3** and the naphthalene aza scorpiand **L4**. The distribution diagrams of **L1** and **L2** are collected in Figures 1 and S1 (Supporting Information), respectively.

Both **L1** and **L2** present in the pH range of study (2.5−11.0) three relatively high stepwise constants separated by *ca.* 1.5 logarithmic units and a much lower fourth constant. Interestingly, the first three stepwise basicity constants of **L1** and particularly of **L2** are lower than the corresponding ones of **L3**, which can be in part attributed to the electron withdrawing characteristics of the pyridine rings and to the fact that **L3** contains a primary amino group in the tail that has more favorable hydration energy.[23] ^{1}H and ^{13}C NMR data can give indications of the protonation sequence followed by polyamine ligands since it is well-known that upon protonation, the hydrogen nuclei bound to the α-carbon and the carbon nuclei in the β position with respect to the nitrogen atoms bearing the protonation processes are those experiencing, respectively, the largest downfield and upfield shifts.[24]

The variation of the ^{1}H signals of protons H1 and H6 (for the labeling, see Chart 1), which are respectively placed in the α position with respect to the secondary nitrogen atoms of the macrocyclic core and of the tail, are particularly relevant in this respect (Figure 2, bottom). In the case of **L1**, H1 undergoes, in correspondence with the first two protonation steps (pH 11.35 down to pH 7.81), a much larger downfield shift (H1, $\Delta\delta$ = 0.56 ppm) than H6 ($\Delta\delta$ = 0.13 ppm), suggesting that these two protonations occur at a larger extent at the secondary amino groups of the macrocyclic core. However, it has to be emphasized that ^{1}H NMR reflects an average situation, and protonation

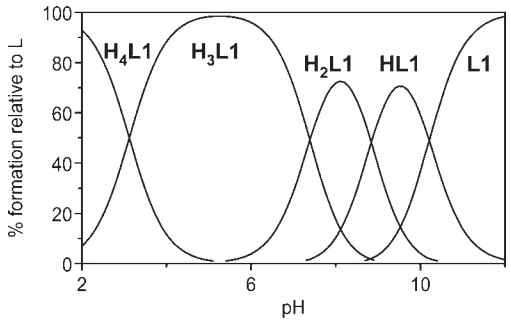

Figure 1. Distribution diagram for receptor **L1**.

at some extent of the secondary nitrogen atom of the tail should also be occurring.

The chemical shifts of H1 and H6 have opposite variations when the third protonation occurs; from pH 7.81 to 5.76, while a $\Delta\delta$ of 0.41 ppm is found for proton H6, the signal of proton H1 experiences a $\Delta\delta$ of just 0.14 ppm (Figure 2, bottom), indicating a preferential protonation of the secondary nitrogen atom of the tail. These results differ from those previously reported for **L3**, in which first protonation occurred preferentially at the primary nitrogen of the tail. This can be attributed to the more favorable solvation energy of the primary amino group in water. However, the preferential protonation of the secondary nitrogen atoms of the macrocycle in **L1** agrees with the protonation pattern previously inferred using a variety of techniques for **L4**, which contains a naphtylmethyl group in the tail.[7]

Protonation of the pyridine nitrogen is evidenced by the shifts experienced by all of the ^{1}H signals of the pyridine ring of the tail in the pH range 5.8−1.8. While, in this pH region, the doublet signal attributable to hydrogen atoms py2 and the triplet signal of hydrogens py3 do not undergo significant changes, all of the proton signals of the pyridine ring at the tail bear significant downfield shifts (Hpy3′, $\Delta\delta$ = 0.42 ppm; Hpy4′, $\Delta\delta$ = 0.45 ppm; Hpy5′, $\Delta\delta$ = 0.42 ppm; Hpy6′, $\Delta\delta$ = 0.32 ppm).

In the case of **L2**, the protonation constant of the pyridine at the tail has also been inferred from UV spectroscopy following the changes with pH of the band centered at 260 nm. The value obtained with the HYPERQUAD program[16] (log K = 3.45(2)) agrees quite well with the value of the last protonation step of **L2** determined by pH-metric titrations and supports the proposed protonation pattern for this stage.

The analysis of the different NMR chemical shifts for the receptor **L2** shows a similar pattern to that of L1 (see Figure S2, Supporting Information). Therefore, both macrocycles experience a similar average protonation pattern in which first two protonations preferentially occur at the secondary amino groups of the macrocycle; the third protonation is produced at the secondary amino group of the tails, with a fourth much lower protonation occurring at the nitrogen of the pendant arm pyridine ring. No protonation of the macrocycle pyridine ring is observed in the covered pH interval, probably because its protonation is severely hindered due to its participation in hydrogen bonding with adjacent protonated nitrogens. In any case, it must be emphasized that the conclusions derived only refer to the average protonation sequences.

(23) (a) Bencini, A; Bianchi, A.; García-España, E.; Micheloni, M.; Ramírez, J. A. *Coord. Chem. Rev.* **1999**, *188*, 97–156. (b) Albelda, M. T.; García-España, E.; Jiménez, H. R.; Llinares, J. M.; Soriano, C.; Sornosa-Ten, A.; Verdejo, B. *Dalton Trans.* **2006**, 4474–4481. (c) Sarneski, J. E.; Surprenant, H. L.; Molen, F. K.; Reilley, C. N. *Anal. Chem.* **1975**, *47*, 2116–2124.

(24) (a) Frassineti, C.; Ghelli, S.; Gans, P.; Sabatini, A.; Moruzzi, M. S.; Vacca, A. *Anal. Biochem.* **1995**, *231*, 374–382. (b) Frassineti, C.; Alderighi, L.; Gans, P.; Sabatini, A.; Vacca, A. *Anal. Bioanal. Chem.* **2003**, *376*, 1041–1052. (c) Dagnall, S. P.; Hague, D. N.; McAdam, M. E.; Moreton, A. D. *J. Chem. Soc. Faraday Trans.* **1985**, *81*, 1483–1494. (d) Hague, D. N.; Moreton, A. D. *J. Chem. Soc., Perkin Trans 2: Phys. Org. Chem.* **1994**, *2*, 265–270.

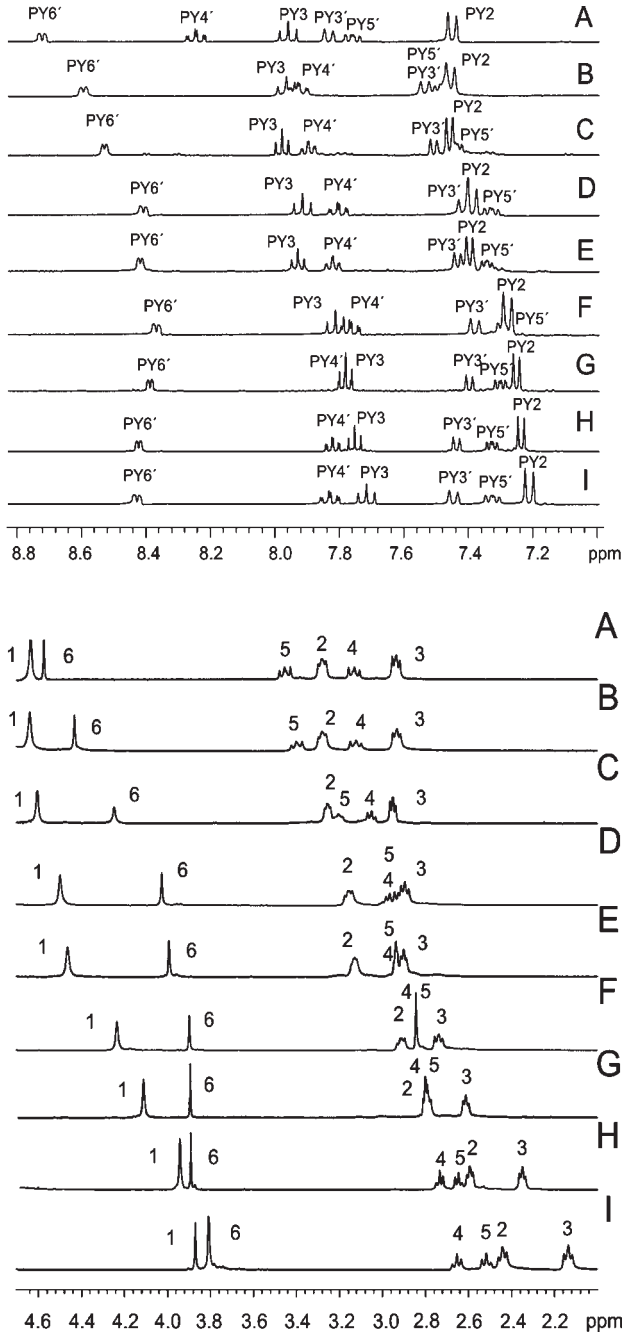

Figure 2. Variation of the ^{1}H NMR spectra of **L1** with pH in the aliphatic (bottom) and aromatic (top) regions: (A) pD = 1.85, (B) pD = 5.76, (C) pD = 7.2, (D) pD = 7.81, (E) pD = 8.6, (F) pD = 9.42, (G) pD = 10.42, (H) pD = 11.35.

The complex structure of the ligands, with multiple protonation sites and hydrogen bonding possibilities, will probably lead to the formation in solution of mixtures of rapidly exchanging isomers with different protonation sites for a given H_xL^{x+} species, and only those isomers achieving larger concentrations contribute significantly to the experimental NMR spectra.

Cu^{2+} Complexation Studies. The formation of Cu^{2+} complexes with **L1** and **L2** was studied both in the solid state and in solution, in the latter case by means of potentiometric titrations and UV−vis spectroscopy. With regard to the solid state structure, crystals of suitable quality could only be obtained for the complex of **L1**. However, the analysis of the titration data provides useful information about the differences in the coordination behavior of both scorpiands.

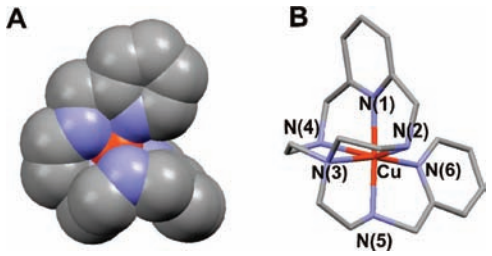

Figure 3. Space filling (A) and stick (B) representations of the $[CuL1]^{2+}$ cation. Hydrogens are not shown.

Crystal Structure of $[CuL1](ClO_4)_2$. The asymmetric unit of the $[CuL1](ClO_4)_2$ structure includes one $[CuL1]^{2+}$ cation and two perchlorate counterions. Figure 3 shows that the coordination geometry around the metal ion is distorted octahedral with significant axial elongation.

The equatorial plane of the octahedron is defined by the pyridine nitrogens of the macrocyclic framework and of the pendant arm and the secondary amino group of the tail, all three distances being close to 2 Å, and the tertiary nitrogen, which displays a slightly longer distance (Cu(1)−N(3) = 2.126 Å, see Table 2). The elongated axial positions are occupied by the secondary nitrogens of the macrocyclic framework, one of these distances being particularly long (Cu(1)−N(4) = 2.376 Å).

Interestingly, the angle in the axial direction departs significantly from 180° (N(2)−Cu(1)−N(4) = 151.7°). The Cu^{2+} ion lies nicely in the equatorial plane with angles that are in the range 81.5−99.1°. As can be seen in the space filling representation of the cation $[CuL1]^{2+}$ (Figure 3A), the copper atom is completely embedded within the cage-like cavity formed by the macrocycle and the pendant arm being completely isolated from the environment. An interesting bit of data is the almost normal angle (99.1°) formed by the pyridine rings at the macrocyclic framework and the tail.

Cu^{2+} Speciation Studies. pH-metric titrations carried out at 298.1 K in 0.15 M $NaClO_4$ gave the model species and stability constants collected in Table 3 for the systems Cu^{2+}−**L1** and Cu^{2+}−**L2**. Table 3 also includes for comparative purposes the literature results for the systems Cu^{2+}−**L3** and Cu^{2+}−**L4**.

Direct titrations of Cu^{2+} and $H_3L1\cdot 3HCl$ aqueous solutions with a base gave a value of the stability constants of the $[CuL1]^{2+}$ species of *ca.* 22.8(1) logarithmic units. However, the stability of the complex is so high that the fitting could only be performed with points belonging to a very acidic region. A distribution diagram recorded for a 1:1 Cu^{2+}/**L1** molar ratio ($[Cu^{2+}] = 10^{-3}$ M) shows that 92% of the $[CuL1]^{2+}$ is already formed at pH = 3, and at pH = 3.5, $[CuL1]^{2+}$ is quantitatively formed. Therefore, to check these results, a competition method in which solutions containing Cu^{2+} and both **L1** and the parent ligand **L3** were titrated with base was performed. Treatment of the mixed system with the HYPERQUAD program[16] taking the constants of the system Cu^{2+}−**L3** as fixed parameters gave a stability constant value of $[CuL1]^{2+}$ of 22.6(1) (Table 3) logarithmic units, which is in good agreement

Table 2. Selected Both Lengths (Å) and Angles (deg) for Compound [Cu**L1**](ClO$_4$)$_2$

Bond Distances			
Cu(1)−N(1)	2.025(9)	Cu(1)−N(5)	1.976(10)
Cu(1)−N(6)	2.015(9)	Cu(1)−N(2)	2.20(3)
Cu(1)−N(3)	2.126(10)	Cu(1)−N(4)	2.376(15)
Bond Angles			
N(1)−Cu(1)−N(2)	80.4(9)	N(2)−Cu(1)−N(5)	98.0(11)
N(1)−Cu(1)−N(3)	92.9(3)	N(3)−Cu(1)−N(4)	77.7(7)
N(1)−Cu(1)−N(5)	178.2(12)	N(3)−Cu(1)−N(5)	86.0(6)
N(8)−Cu(1)−N(11)	80.5(8)	N(3)−Cu(1)−N(6)	168.0(4)
N(1)−Cu(1)−N(6)	99.1(4)	N(4)−Cu(1)−N(5)	102.9(10)
N(2)−Cu(1)−N(4)	151.6(5)	N(4)−Cu(1)−N(6)	104.2(8)
N(2)−Cu(1)−N(6)	97.8(10)	N(5)−Cu(1)−N(6)	81.5(4)

Table 3. Logarithms of the Formation Constants of Cu^{2+} Complexes with **L1** and **L2** Determined in 0.15 M $NaClO_4$ at 298.1 K

reaction[a]	**L1**	**L2**	**L3**[c]	**L4**[c]
Cu + 2H + L ⇆ CuH_2L		25.59(2)[b]		
Cu + H + L ⇆ CuHL		21.91(3)	24.28(2)	22.65(2)
Cu + L ⇆ CuL	22.6(1)	17.68(4)	20.43(3)	19.65(4)
Cu + L + H_2O ⇆ CuL(OH) + H		7.27(5)	9.42(3)	
CuHL + H ⇆ CuH_2L		3.68(4)		
CuL + H ⇆ CuHL		4.23(5)	3.85(3)	3.00(2)
CuL + H_2O ⇆ CuL(OH) + H		−10.41(8)	−11.01(3)	

[a] Charges omitted. [b] Values in parentheses are standard deviations in the last significant figure. [c] Taken from ref 7.

with the value obtained from the direct titrations. This value of the stability constant is higher than those calculated for **L2**, **L3**, and **L4** (Table 3) and supports the conclusion that the hexa-coordination observed in the crystal structure is also attained in solution. The absence of any hydroxylated species also gives support to the completion of the coordination sphere of Cu^{2+} by the six nitrogen donor of the ligand.

In the case of the system Cu^{2+}−**L2**, apart from observing a [Cu**L2**]$^{2+}$ species of significantly lower stability (Table 3), two protonated species ([CuH**L2**]$^{3+}$ and [CuH_2**L2**]$^{4+}$) and a hydroxylated species ([Cu**L2**(OH)]$^{+}$) are also detected in the pH-metric titrations. These results indicate that the position of the pyridine nitrogen in **L2** prevents its coordination to the metal ion. Moreover, the low value of the formation of [Cu**L2**]$^{2+}$ may even suggest that the secondary nitrogen in the tail does not coordinate, which could also explain the higher tendency of this complex to become protonated with respect to the **L1** analogue. The protonation steps of [Cu**L2**]$^{2+}$ can be ascribed to the protonation of the pyridine nitrogen of the tail and to the protonation of the secondary amino group of the pendant arm; the former protonation could occur without any disruption of the coordination sphere of the metal ion. The remaining positions in the coordination sphere of [Cu**L2**]$^{2+}$ should be occupied by water molecules, which could hydrolyze to give the [Cu**L2**(OH)]$^{+}$ species

Kinetic Studies. To check the possible differences in the kinetic properties of the metal complexes formed by **L1** and **L2**, kinetic studies were carried out both on complex formation and complex decomposition. In addition to the complexation-decomplexation processes, those kinetic studies were expected to provide also information about the possible occurrence in these complexes of the molecular movement typical of scorpiands.

Kinetics of Decomposition of the Cu^{2+} Complexes. As occurs in general for metal−polyamine complexes, the addition of an excess of acid to a solution of the metal complexes must result in complex decomposition with the release of free Cu^{2+} and the protonated ligand **L1** or **L2** according to eq 1.

$$[CuL]^{2+} + H^{+}_{exc} \rightarrow Cu^{2+} + H_xL^{x+} \quad (1)$$

Solutions containing Cu^{2+} and the macrocycle in a 1:1 molar ratio with the pH adjusted to the value required for complete formation of the corresponding [CuL]$^{2+}$ complex were mixed with an excess of acid and the spectral changes registered with either a stopped-flow instrument or a conventional spectrophotometer. The results indicate that the decomposition of the Cu^{2+} complexes with both ligands occurs with significantly different kinetics.

Decomposition of the complex with **L1** occurs with a single kinetic step in which the spectra show the disappearance of the typical band of the complex centered at 640 nm. The observed rate constants show a linear dependence (Figure 4) with respect to the acid concentration, and the data can be fitted satisfactorily by eq 2 with $a = (9.7 \pm 0.1) \times 10^{-4}$ M^{-1} s^{-1}.

$$k_{obs} = a[H^{+}] \quad (2)$$

These results can be easily rationalized assuming the mechanism proposed by Margerum et al. for the decomposition of metal chelates,[26] for which there is an initial formation of an activated intermediate with an elongated Cu−N bond. Although this intermediate is susceptible to attack by the solvent or a proton, the absence of a nonzero intercept in Figure 4 indicates that in this case the complex decomposes exclusively through the proton-assisted pathway. In this sense, it can be pointed out that the relative importance of the H_2O and H^+ pathways has been proposed to depend on the type of chelate rings formed, the H_2O pathway being more important when six-member chelate rings are formed.[27]

The kinetics of decomposition of the [Cu**L2**]$^{2+}$ complex are more complicated because when solutions of the complex are mixed in the stopped-flow instrument with an excess of acid, the spectrum recorded immediately upon mixing does not show the band of the [Cu**L2**]$^{2+}$ species but a band centered at 690 nm, which corresponds with the spectrum recorded for solutions containing [CuH**L2**]$^{3+}$ (see Figure 5). These results demonstrate that decomposition of the complex occurs with biphasic kinetics, as indicated in eqs 3−5. The first step is too fast for its rate constant (k_{1obs}) to be measured even with the stopped-flow technique (mixing time of *ca.* 1.7 ms for the instrument used), and it leads to the formation of a [CuH**L2**]$^{3+}$ intermediate with absorption spectra similar to that of the [CuL]$^{2+}$ complex of the related macrocyclic ligand lacking the pendant arm, which indicates that dissociation of the amino group

(25) Gilli, P.; Pretto, L.; Bertolasi, V.; Gilli, G. *Acc. Chem. Res.* **2009**, *42*, 33–44.
(26) (a) Read, R. A.; Margerum, D. W. *Inorg. Chem.* **1981**, *20*, 3143–3149. (b) Margerum, D. W.; Cayley, G. R.; Weatherburn, D. C.; Pagenkopf, G. K. *ACS Monography* **1978**, 174.
(27) Chen, L. H.; Chung, C. S. *Inorg. Chem.* **1989**, *28*, 1402–1405.

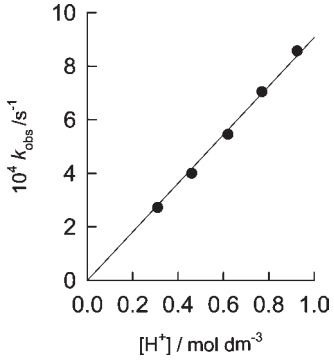

Figure 4. Plot of the dependence on the acid concentration of the observed rate constant for the acid-promoted decomposition of the $[CuL1]^{2+}$ complex ($[NaClO_4] = 1.0$ M, 298.1 ± 0.1 K).

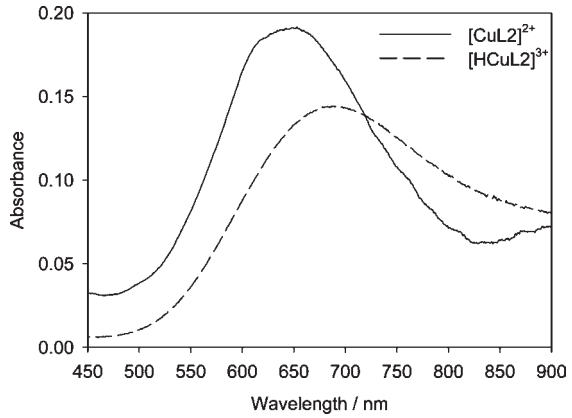

Figure 5. Electronic spectra for aqueous solutions containing the $[CuL2]^{2+}$ and $[CuHL2]^{3+}$ complexes.

in the pendant arm is very rapid and is signaled by a measurable shift in the absorption spectrum. Some attempts were also made to obtain information about the kinetics in the first step using pH-jump strategies, but those experiments were unsuccessful because the process is too fast for the stopped-flow technique under all the experimental conditions tried. In contrast, the second step is slow enough to be monitored with a conventional spectrophotometer, and it leads to complete decomposition of the complex. The spectral changes can be fitted satisfactorily by a single exponential to obtain k_{2obs} values that show a second-order dependence with respect to the acid concentration (see Figure 6), and the experimental points can be fitted by eq 5 with $c = (8 \pm 2) \times 10^{-5}$ s^{-1} and $b = (7.4 \pm 0.4) \times 10^{-4}$ M^{-2} s^{-1}. Although most Cu−polyamine complexes decompose with first-order kinetics with respect to the acid concentrations, there are several examples in the literature of second-order dependence, which is usually interpreted as being a consequence of the displacement of the rate determining step from the breaking of the first Cu−N bond to the second one.[28−32] Regarding

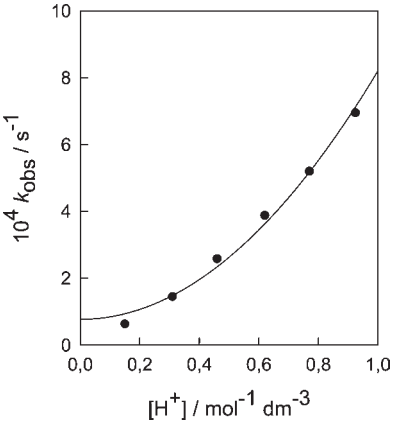

Figure 6. Plot of the dependence on the acid concentration of the observed rate constant for the acid-promoted decomposition of the $[CuHL2]^{3+}$ complex ($[NaClO_4] = 1.0$ M, 298.1 ± 0.1 K).

the different kinetics of decomposition observed for the complexes with **L1** and **L2**, they appear to be associated with the capability of the **L2** complex to evolve rapidly to a stable protonated intermediate upon acid attack, in agreement with the results of the potentiometric studies.

$$[CuL]^{2+} + H^+ \rightarrow CuHL^{3+};\ k_{1obs} \quad (3)$$

$$[CuHL]^{3+} + H^+_{exc} \rightarrow Cu^{2+} + H_xL^{x+};\ k_{2obs} \quad (4)$$

$$k_{2obs} = c + b[H^+]^2 \quad (5)$$

Kinetics of Formation of the Cu^{2+} Complexes. In order to make complex formation slow enough to be measured with the stopped-flow instrument, kinetic studies on complex formation had to be carried out under non-pseudo-first-order conditions, i.e., using stoichiometric concentrations of the metal ion and the ligand, and in moderately acidic media (pH = 2−6) without adding buffer systems to the solutions because the addition of buffers has been shown to introduce some complications.[33] Under these conditions, Cu^{2+} exists solely as the aqua complex, and the kinetic data are not complicated by any contribution from Cu^{2+} hydroxo complexes to the rate of reaction. Moreover, as **L1** and **L2** are highly protonated at low pH, this makes the equilibrium constants for the formation of the outher-sphere complexes with Cu^{2+} small enough to make possible kinetic studies on the formation of Cu^{2+}−L complexes. However, the absence of buffers in the kinetic measurements makes the H^+ concentration change during complex formation. For this reason, the data were fitted with the programs SPECFIT[17] and Pro-Kineticist II[34] to take into account these changes in $[H]^+$ and to analyze globally all measurements made at different starting pH values. The data for an experiment at a given starting pH value were initially fitted using the program SPECFIT, and the results were then used to analyze globally with Pro-Kineticist II the data corresponding to the whole set

(28) Basallote, M. G.; Duran, J.; Fernandez-Trujillo, M. J.; Mañez, M. A. *J. Chem. Soc., Dalton Trans.* **2002**, 2074–2079.
(29) Curtis, N. F.; Osvath, S. R. *Inorg. Chem.* **1988**, *27*, 305–310.
(30) Hay, R. W.; Bembi, R.; Moodie, W. T.; Norman, P. R. *J. Chem. Soc., Dalton Trans.* **1982**, 2131–2136.
(31) Hay, R. W.; Pujari, M. P.; McLaren, F. *Inorg. Chem.* **1984**, 3033–3035.
(32) Hay, R. W.; Tarafder, M. T. H.; Hassan, M. M. *Polyhedron* **1996**, 725–732.
(33) (a) Maeder, M.; Neuhold, Y. M.; Puxty, G.; King, P. *Phys. Chem. Chem. Phys.* **2003**, *5*, 2836–2841. (b) Basallote, M. G.; Duran, J.; Fernandez-Trujillo, M. J.; Manez, M. A.; Szpoganicz, B. *J. Chem. Soc., Dalton Trans.* **1999**, 1093–1100.
(34) Puxty, G.; Maeder, M.; Neuhold, Y.-M.; King, P. *Pro-Kineticist II*; Applied Photophysics, Ltd.: Leatherhead, England, 2001.

Table 4. Mechanistic Model and Rate Constants for the Formation of Cu^{2+} Complexes with **L1** and **L2**

ligand (reactive species)	reactions leading to complex formation	rate constants
L1 (H_3L^{3+})	$H_3L^{3+} + Cu^{2+} \rightarrow [(CuL)^{2+}]^* + 3H^+$; $k_{Cu,H3L1}$	$k_{Cu,H3L1} = (6.70 \pm 0.02) \times 10^3\ M^{-1}\ s^{-1}$
	$[(CuL)^{2+}]^* \rightarrow (CuL)^{2+}$; k_{2CuL1}	$k_{2CuL1} = (1.24 \pm 0.05) \times 10^{-1}\ M^{-1}\ s^{-1}$
L2 (H_2L^{2+})	$H_2L^{2+} + Cu^{2+} \rightarrow (CuL)^{2+} + 2H^+$; $k_{Cu,H2L2}$	$k_{Cu,H2L2} = (8.14 \pm 0.02) \times 10^2\ M^{-1}\ s^{-1}$

of different experiments. During the refinement process all the protonation equilibria revealed by the potentiometric measurements were considered with the corresponding equilibrium constants fixed at the values shown in a previous section. The best fit of the whole set of experimental data for each ligand was achieved with the models shown in Table 4.

An important difference between both ligands is that the only protonated ligand species that leads to formation of the $[Cu\mathbf{L1}]^{2+}$ complex is H_3L^{3+}, whereas for $[Cu\mathbf{L2}]^{2+}$ it is H_2L^{2+}. Although H_4L^{4+} exists in noticeable concentrations in the pH range covered in the kinetic studies, its contribution to the observed rate constant is negligible. It must also be stated that formation of the $[Cu\mathbf{L1}]^{2+}$ complex occurs with the formation of a detectable reaction intermediate whose calculated electronic spectrum is shown in Figure 7, although its precise nature cannot be established unequivocally because the quality of the fit of kinetic data to models including two or three released protons in the first step are similar. On the other hand, the fact that the reaction of Cu^{2+} with the triprotonated form of **L1** is faster than with diprotonated **L2** is surprising from an electrostatic point of view, but it must be considered that the complex structure of the ligands can lead to very different distributions of the positive charges, which can result in rate constants that do not follow the trends usually observed for simpler ligands. This point will be addressed with more details in the DFT section below.

With regard to the comparison of the present kinetic results with those previously reported for the related **L3** and **L4** complexes, it must be pointed out that the rate of complex formation between Cu^{2+} and the $H_3\mathbf{L1}^{3+}$ species is 4 orders of magnitude higher than with the corresponding species of **L3** and **L4**. This finding can be explained by the existence in **L1** of one additional nitrogen atom that facilitates the beginning of complex formation. In contrast, $H_3\mathbf{L3}^{3+}$ and $H_3\mathbf{L4}^{3+}$ contain two protons at the macrocycle, and the additional proton is located on the amino group at the side chain,[7] so that there are not unprotonated nitrogen atoms not involved in intramolecular hydrogen bonding and with the orientation required to interact with Cu^{2+}, thus resulting in a slower reaction. On the other hand, the rate constant for the reaction of Cu^{2+} with $H_2\mathbf{L2}^{2+}$ is almost an order of magnitude higher than that observed for reaction with the same protonated form of the macrocyclic ligand lacking a side chain.[7] This modest acceleration can be understood by considering that the higher rate resulting from the introduction of two additional potential donors in the side chain will be partially balanced by the higher steric hindrance in $H_2\mathbf{L2}^{2+}$ and by the possible participation of those donors in the hydrogen bonding network.

Regarding the mechanism of formation of the $Cu^{2+}-\mathbf{L}$ complexes, it is widely accepted that complexation of a metal ion by a monodentate ligand in aqueous solution occurs according to the Eigen−Wilkins mechanism (eqs 6−8).

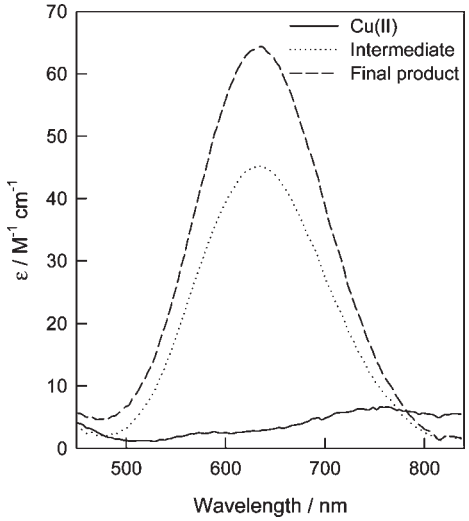

Figure 7. Electronic spectra calculated for the different species involved in the formation of the $[Cu\mathbf{L1}]^{2+}$ complex.

$$M(H_2O)_6^{z+} + L \leftrightarrows \{M(H_2O)_6^{z+}, L\}_{os};\ K_{os} \quad (6)$$

$$\{M(H_2O)_6^{z+}, L\}_{os} \rightarrow \{M(H_2O)_5L^{z+} + H_2O\};\ K_{M\text{-}H2O} \quad (7)$$

$$K_{obs} \approx K_{os} \times K_{M\text{-}H2O}[L] \quad (8)$$

The first step involves the interaction of the aquated metal ion with the ligand to form an outer-sphere complex in an essentially instantaneous equilibrium quantitatively defined by the outher-sphere stability constant K_{os}. The second step is a ligand-exchange reaction where one coordinated water molecule is replaced by the entering ligand. The rate law for this mechanism is given by eq 8 if the equilibrium in eq 6 is considered to be displaced to the left-hand side, as occurs frequently in water solutions. The values of the second-order rate constant are usually in good agreement with the theoretical values calculated from the product $K_{os} \times k_{M\text{-}H2O}$ (eq 8), where K_{os} is obtained using the Fuoss equation and $k_{M\text{-}H2O}$ represents the rate constant for solvent exchange.[35,36] For polydentate ligands, the mechanism can be more complicated because complex formation involves several consecutive substitutions and the rate-determining step can be displaced to the formation of one of the subsequent bonds. However, rate-determining formation of the first bond followed by a subsequent rapid ring closure is the most

(35) Wilkins, R. G. *Kinetics and Mechanism of Reactions of Transition Metal Complexes*, 2nd ed.; VCH Publications: Weinheim, Germany, 1991; Chapter 4.

(36) Fuoss, R. M. *J. Am. Chem. Soc.* **1958**, *80*, 5059–5061.

Table 5. Kinetic and Mechanistic Data for Formation of Cu^{2+}–**L** Complexes[a]

ligand reactive species	$k_{Cu,HxL}$ (M^{-1} s^{-1})	K_{OS} (M^{-1})	k_{theor} ($M^{-1}s^{-1}$)	$k_{Cu,HxL}/k_{theor}$	ρ_{theor}	ρ_{exp}
H_3**L1**$^{3+}$	$(6.70 \pm 0.02) \times 10^3$	1.1×10^{-3}	8.7×10^6	7.7×10^{-4}	0.018–0.058	1.0×10^{-3}
H_2**L2**$^{2+}$	$(8.14 \pm 0.08) \times 10^2$	7.4×10^{-3}	5.8×10^7	1.4×10^{-5}	0.036–0.064	1.8×10^{-5}

[a] The meaning of the different parameters is defined in the text.

common situation for most polydentate ligands. The formation of the second (or latter) bond rate-determining step only occurs in cases where the first step is unusually rapid or when steric hindrance or strain inhibit ring closure.[35] In the latter cases, accumulation of the intermediate with the polydentate ligand acting monodentate is expected. For the systems studied in the present work, kinetic experiments indicate that the initial spectrum in the stopped-flow experiments on complex formation coincides with that of the Cu^{2+} aqua complex, so that formation of the first metal–ligand bond can be reasonably considered the rate-determining step.

In that case, the rate constants for complex formation with the H_3**L1**$^{3+}$ and H_2**L2**$^{2+}$ species are expected to be close to the values estimated by using eq 8, the Fuoss treatment to estimate K_{OS},[37,38] and the rate constant for water exchange in the Cu^{2+} aqua complex. The resulting values (k_{theor}) are included in Table 5 together with the corresponding experimental values ($k_{Cu,HxL} = k_{Cu,H3L1}$, $k_{Cu,H2L2}$) and the quotient between them. The values of the $k_{Cu,HxL}/k_{theor}$ ratio indicate that the rate constants for complex formation are several orders of magnitude smaller than the values predicted by eq 8. Although the Fuoss treatment is probably an oversimplification because it considers the metal ion and the ligand as charged points and the size of reactants is only taken into account to establish the distance at the point of closest approach, these differences cannot be ascribed to a general failure of the model because Secco and co-workers have found good agreement between experimental and theoretical values for the formation of Cu^{2+} complexes with different protonated forms of several polydentate polyamine ligands.[38]

An important limitation of this model is that the Fuoss equation considers the species as a charged point without considering the disposition of the donor atoms. To solve this problem, Rorabacher proposed years ago a treatment in which ligands are considered as "donor atoms with a tail", introducing a steric factor (ρ) whose values are considered to be additive for the different potential donor atoms available since complex formation can start with the coordination of any of them. Table 5 includes theoretical values of the steric parameter (ρ_{theor}) calculated by the addition of the contributions corresponding to the different types of donor nitrogens available in the H_3**L1**$^{3+}$ and H_2**L2**$^{2+}$ species.[39,40] As there is some uncertainty about the actual nature of the unprotonated groups in those species, ranges of ρ_{theor} values that cover the different possibilities are given in Table 5. Those theoretical values can be compared with those calculated from the experimental values (ρ_{exp}) of the rate constants using eq 9.

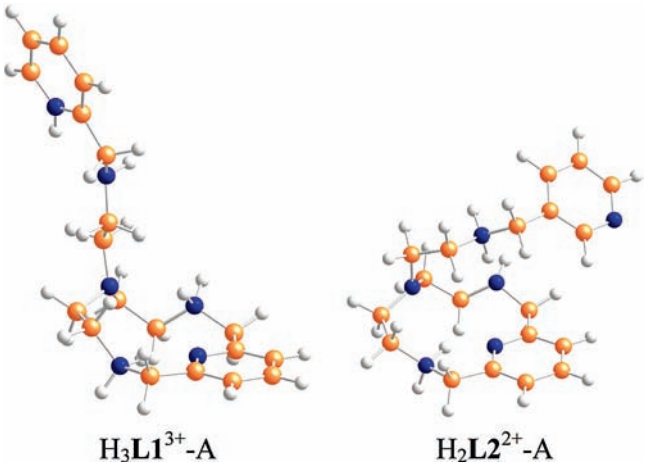

Figure 8. Optimized geometries for the conformations of the protonated forms of **L1** and **L2** ligands leading to complex formation.

$$k = \frac{3}{4} K_{os} \times k_{M-H2O} \times \rho \qquad (9)$$

This comparison reveals that the experimental values are still 1–3 orders of magnitude smaller than the theoretical ones. Although this can be interpreted as being indicative of a change in the rate-determining step from the formation of the first metal–ligand bond to the formation of one of the subsequent bonds, conformational changes must also be taken into account because they can play an important role in the process of complex formation. In general, the treatment of ligands as "donor atoms with a tail" seems to be too simple for species as structurally complex as scorpiands, in which extensive intramolecular hydrogen bonding is expected, and it should lead to a reduction in the number of free donor atoms available for complex formation.[7] To obtain additional information about the effect of the conformation of the ligands in complex formation, some DFT studies were carried out, and they proved to be very useful to understand the kinetic results for complex formation and to confirm the important role in those processes of the formation of intramolecular hydrogen bonds. Those studies also provided some information about another interesting point in the mechanism of formation of these kinds of complexes, i.e., the role of donor atoms in the pendant arm of the scorpiand.

DFT Calculations. Since the experimental data in previous sections indicate that the reactive protonated form in complex formation is H_3L^{3+} for **L1** and H_2L^{2+} for **L2**, the theoretical DFT calculations were focused on these species. However, the H_4L^{4+} species were also studied because they are also major species in solution in the pH range covered in the kinetics studies. For determining the possible conformations that **L1** and **L2** can adopt

(37) Eigen, M.; Kruse, W.; Maass, G.; Demaeyer, L. *Progr. React. Kinet. Mech.* **1964**, *2*, 285.
(38) Biver, T.; Secco, F.; Tine, M. R.; Venturini, M. *Polyhedron* **2001**, *20*, 1953–1959.
(39) Rorabacher, D. B.; Melendez-Cepeda, C. A. *J. Am. Chem. Soc.* **1971**, *93*, 6071–6076.
(40) Ambundo, E. A.; Deydier, M. V.; Ochryowycz, L. A.; Rorabacher, D. B. *Inorg. Chem.* **2000**, *39*, 1171–1179.

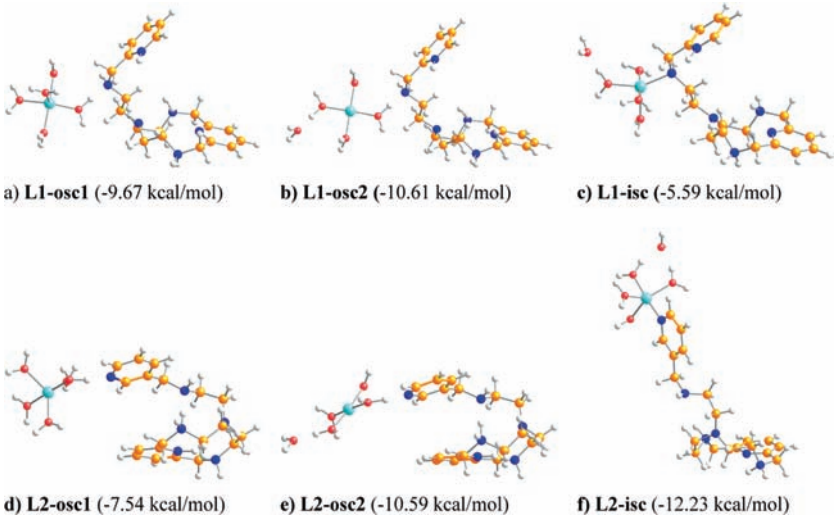

Figure 9. Geometries optimized in water solution for the outer-sphere and inner-sphere complexes with a single Cu−N bond found for the formation of Cu^{2+} complexes with the H_3**L1**$^{3+}$ and H_2**L2**$^{2+}$ species. The energy values are relative to the separated $Cu(H_2O)_5^{2+}$ and the corresponding protonated ligand species. Color code: Cu (turquoise); O (red); N (blue); C (orange); H (white).

depending on the protonation state, multiple optimizations were carried out, and the results are commented upon in more detail in the Supporting Information. In summary, it must be stated that the results of those calculations are in full agreement with the kinetic data. Thus, the calculations indicate that complex formation is not possible directly from the H_4L^{4+} species of either ligand because of the lack of available nitrogen atoms. In the case of **L1**, the analysis of the most stable conformations for the di- and triprotonated species reveals that complex formation is not possible from the most stable conformations of H_2**L1**$^{2+}$, and so, complexation is expected to occur through reaction of the species labeled H_3**L1**$^{3+}$−A (see geometry in Figure 8). In contrast, the diprotonated species labeled H_2**L2**$^{2+}$−A in Figure 8 contains an unprotonated nitrogen at the pyridine ring which is not involved in intramolecular hydrogen bonding, and so it is able to react with Cu^{2+}. It is also interesting to note that the only nitrogen atoms available for coordinating Cu^{2+} in both structures of Figure 8 are located in the pendant arms of both ligands, so that complex formation must start at those positions and incorporation to the macrocyclic ring must occur at a later stage. Of particular relevance is the case of the pyridine nitrogen at the side chain of **L2**: although its orientation hinders simultaneous coordination with the donors at the macrocyclic subunit, it allows for the initial interaction with the metal ion, so that this donor group acts as bridgehead for complexation, which should be completed through a molecular reorganization process in which Cu^{2+} is transferred from that pyridine group to the macrocycle.

Once established the most stable conformations of the protonated forms of the ligands that lead to complex formation, calculations were also made to obtain information about the details of the reaction pathway leading to complex formation. Because complete formation of the [Cu**L1**]$^{2+}$ and [Cu**L2**]$^{2+}$ complexes is exceedingly complicated to model, the calculations focused on the formation of the first Cu−N bond. However, some comment must be made at this point on the limitations of the DFT

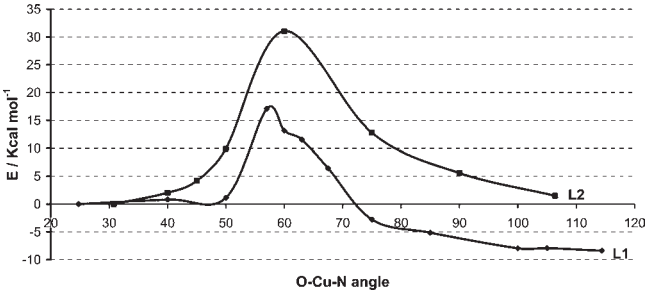

Figure 10. Energy profiles for the formation of inner-sphere complexes with the **L1** and **L2** ligands obtained from scan calculations in water solution.

methodology used.[40−44] Thus, the energy values for the different Cu-containing species must be considered only approximate because the B3LYP functional favors lower coordination numbers by typically 10−55 kJ/mol, thus favoring the I_d/D substitution mechanisms over I_a/A.[40] In fact, recent studies on the water exchange reaction between coordination shells around metal ions in aqueous solution have highlighted that the employed methodology can lead to different results.[44−47] A representative example of the current difficulties is the absence of agreement on the coordination number of Cu^{2+} in water solution.[48−53]

(41) Rotzinger, F. P. *J. Phys. Chem. B* **2005**, *109*, 1510–1527.
(42) Helm, L.; Merbach, A. E. *Coord. Chem. Rev.* **1999**, *187*, 151–181.
(43) Erras-Hanauer, H.; Clark, T.; van Eldik, R. *Coord. Chem. Rev.* **2003**, *238*, 233–253.
(44) Rotzinger, F. P. *Chem. Rev.* **2005**, *105*, 2003–2037.
(45) Berces, A.; Nukada, T.; Margl, P.; Ziegler, T. *J. Phys. Chem. A* **1999**, *103*, 9693–9701.
(46) Pavelka, M.; Burda, J. V. *Chem. Phys.* **2005**, *312*, 193–204.
(47) Rotzinger, F. P. *J. Am. Chem. Soc.* **1997**, *119*, 5230–5238.
(48) Persson, I.; Persson, P.; Sandstrom, M.; Ullstrom, A. S. *J. Chem. Soc., Dalton Trans.* **2002**, 1256–1265.
(49) Pasquarello, A.; Petri, I.; Salmon, P. S.; Parisel, O.; Car, R.; Toth, E.; Powell, D. H.; Fischer, H. E.; Helm, L.; Merbach, A. E. *Science* **2001**, *291*, 856–859.
(50) Schwenk, C. F.; Rode, B. M. *Chem. Commun.* **2003**, 1286–1287.
(51) Schwenk, C. F.; Rode, B. M. *J. Chem. Phys.* **2003**, *119*, 9523–9531.
(52) Blumberger, J.; Bernasconi, L.; Tavernelli, I.; Vuilleumier, R.; Sprik, M. *J. Am. Chem. Soc.* **2004**, *126*, 3928–3938.
(53) Benfatto, M.; D'Angelo, P.; Della Longa, S.; Pavel, N. V. *Phys. Rev. B* **2002**, *65*, 174205.

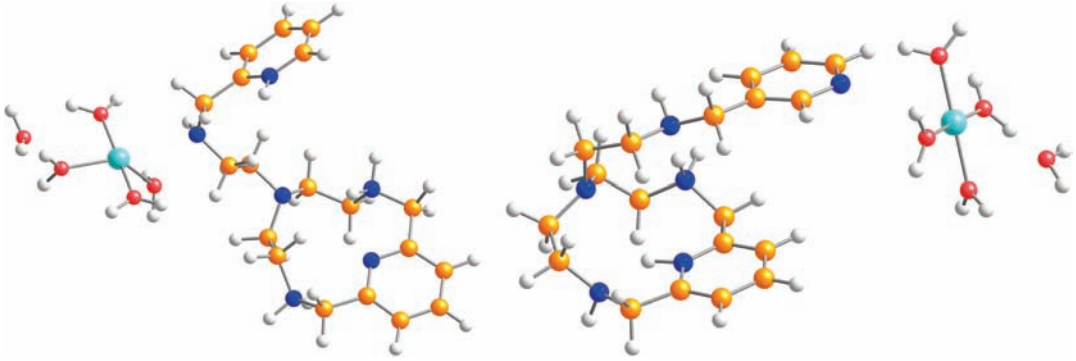

Figure 11. Geometries for the maxima found in the scan calculations for the formation of inner-sphere complexes with the **L1** (left) and **L2** (right) ligands. Color code: Cu (turquoise); O (red); N (blue); C (orange); H (white).

Persson et al.[48] have reported experimental evidence from an EXAFS study that this ion is six-coordinated in aqueous solution, but these results are not consistent with a study carried out by Merbach et al. in which they provide experimental (neutron diffraction)[49] and theoretical results (CPMD calculations),[54,55] indicating a coordination number of five. In the present calculations on the formation of the **L1** and **L2** complexes, penta-coordinated copper has been employed as a model of aqueous Cu^{2+}, and the calculations determined the viability of reaction pathways involving the $H_3\mathbf{L1}^{2+}$−A and $H_2\mathbf{L2}^{3+}$−A species in Figure 8. Nevertheless, alternative reaction pathways involving other conformers cannot be ruled out.

Optimization of $H_3\mathbf{L1}^{2+}$−A and $H_2\mathbf{L2}^{3+}$−A with the $[Cu(H_2O)_5]^{2+}$ ion placed in the vicinity of the HOMO of these species leads to the outer-sphere complexes **L1-osc1** and **L2-osc1** (Figure 9a and d, respectively). In both cases, the electron pair at the nitrogen atom is pointing at one of the hydrogen atoms of a coordinated water molecule, thus leading to a hydrogen-bonding interaction. The relative energies of these adducts with respect to the separate reagents are −9.67 and −7.54 kcal mol^{-1}, in agreement with the formation of a typical hydrogen bond.[25]

The next step in Cu−N bond formation must be the substitution by the organic ligand of one axial water molecule through a transition state that connects it with the final products.[38,56] However, all attempts to find that transition state for the direct replacement were unsuccessful. On the other hand, as previous results by Rotzinger[41,44] on first row transition metals indicate that the dissociative pathway is the only possible one for water exchange in the case of Cu^{2+}, the possibility of such a mechanism was tested for the present systems. In this way, the most stable structures found after dissociation of a water molecule in **L1-osc1** and **L2-osc1** are **L1-osc2** and **L2-osc2** (Figure 9b and e, respectively). These structures show that dissociation of the axial water molecule is the most energetically favorable dissociative process, in agreement with the commonly assumed mechanism.[38,56] These outer-sphere species can be considered square-planar $[Cu(H_2O)_4]^{2+}$ complexes which are hydrogen-bonded to the dissociated water molecule and the corresponding organic ligand. These adducts are slightly more stable than the corresponding penta-coordinated ones, 0.94 and 3.05 kcal mol^{-1} for the **L1** and **L2** ligands, respectively, therefore showing that dissociation of a coordinated water molecule to form a hydrogen-bonding network with the primary solvation shell is thermodynamically favored. These results are also in good agreement with theoretical calculations carried out by Ziegler et al. on the solvation of $Cu(H_2O)_n^{2+}$ and $Cu(NH_3)_n^{2}$ ($n = 3-8$) species by static DFT and *ab initio* molecular dynamics simulations, where they found that as the number of solvent molecules increases to more than four, the additional ligands prefer to be hydrogen-bonded to the planar tetragonal primary hydration shell of $[Cu(solvent)_4]^{2+}$ instead of filling a vacant axial position.[45]

Following the process of complex formation, for both ligands it was possible to obtain final substitution products with a Cu−N bond. Regarding the structures of these inner sphere complexes, it must be pointed out that optimizations with a square pyramidal structure, i.e. $[(CuL(H_2O)_4)\cdots(H_2O)]^{2+}$, and an octahedral geometry, i.e. $[CuL(H_2O)_5]^{2+}$, indicated that the square pyramidal structures are favored by 6.39 and 4.21 kcal/mol for **L1** and **L2**, respectively. Therefore, they were considered as the final products (see Figure 9c and f), and it also allows one to keep the 5-fold coordination number of the copper atom as a constant. The relative energies of the substitution products with respect to the separated reacting species are −5.59 and −12.23 kcal mol^{-1}, respectively, which indicates that the formation of these inner-sphere complexes with a single Cu−N bond is also thermodynamically favored.

Unfortunately, optimization in solvent with the CPCM method did not lead to transition states that connect the **L1-osc2** and **L2-osc2** complexes with their respective final products. For this reason, relaxed scan calculations in solvent were performed on both systems (see the Experimental Section). The reaction coordinate was chosen as the angle between the oxygen atom of the water molecule which is initially hydrogen-bonded to the organic ligand, the copper atom, and the hydrogen-bonded nitrogen atom of the organic ligand. As during the substitution process the selected reaction coordinate changes from a value of 30° in the adducts to *ca.* 110° in the final products, several points along the reaction profile could be calculated, and the energy values are shown in Figure 10. Although there are some differences between both scan

(54) Pasquarello, A.; Laasonen, K.; Car, R.; Lee, C.; Vanderbilt, D. *Phys. Rev. Lett.* **1992**, *69*, 1982–1985.
(55) Laasonen, K.; Pasquarello, A.; Car, R.; Lee, C.; Vanderblit, D. *Phys. Rev. B.* **1993**, *47*, 10142–10153.
(56) Moss, D. B.; Lin, C.-T.; Rorabacher, D. B. *J. Am. Chem. Soc.* **1973**, *95*, 5179–5185.

calculations, an overall view indicates that the less stable point along the reaction pathway is close to an angle of 60° for both systems. The geometries corresponding to the maxima in both scans are included in Figure 11; the Cu−N distances corresponding to the bond that is being formed are 2.75 and 2.67 Å for **L1** and **L2**, respectively. On the other hand, the energy barriers for ligand substitution are relatively high and show a large difference between both ligands (17.1 and 31.1 kcal mol^{-1} for **L1** and **L2**, respectively), but it must be pointed out again that these barriers are surely overestimated by the DFT methodology employed. Nevertheless, the calculations indicate that despite the higher positive charge, complex formation from H_3**L1**$^{3+}$ is faster than from H_2**L2**$^{2+}$, in agreement with the kinetic results.

Conclusions

The results obtained for ligands **L1** and **L2**, which only differ in the position of the substituent at the pendant arm, reveal important differences both in the thermodynamic and kinetic properties, thus providing new information about the relevance of molecular movements in the chemistry of Cu^{2+} complexes with this kind of scorpiand ligand. Thus, in the case of the **L2** ligand, the pyridine ring at the side chain is unable to undergo simultaneous coordination with the macrocyclic donors. This behavior is similar to that the previously reported for scorpiands **L3** and **L4**, which lack the pyridine ring at the side chain. In contrast, the chemistry of the Cu^{2+}−**L1** system is dominated by a very stable hexacoordinate complex whose structure has been solved by X-ray methods. With regard to the kinetic properties, significant differences are also found between both ligands in the processes of complex formation and complex decomposition. Whereas decomposition of the Cu^{2+}−**L1** complex occurs in a single kinetic step, for the **L2** complex, there are two resolved kinetic steps with the formation of a detectable reaction intermediate which corresponds to the structure resulting from the movement typical of scorpiands. Surprisingly, complex formation in moderately acidic solutions occurs through the reaction of aqueous Cu^{2+} with the H_3L^{3+} species in the case of **L1** and with H_2L^{2+} in the case of **L2**, the reaction with H_3**L1**$^{3+}$ being faster than that with H_2**L2**$^{2+}$ despite the higher positive charge. This finding has been rationalized by carrying out DFT calculations, which reveal that the reactive forms of the ligands in the process of complex formation change because the different orientation of the pyridine ring at the side chain makes it act as a bridgehead for complex formation only in the case of the H_2L^{2+} species of **L2**. The related H_2**L1**$^{2+}$ species lacks unprotonated nitrogen donors with an orientation adequate for interacting with the metal ion, and so, complex formation is forced to occur through reaction with H_3**L1**$^{3+}$, which shows an "open-tail" conformation in which the secondary amine group at the side arm can interact with Cu^{2+}. In addition, DFT calculations also provide a full picture of the mechanistic pathway leading to complex formation from those protonated ligand species, in particular the formation of the first Cu−N bond through outer-sphere complexation followed by water dissociation to yield new outer-sphere complexes with the geometries adequate for evolving to inner-sphere metal complexes. Nevertheless, formation of outer-sphere complexes with other conformations of the ligand, with the same or different protonation state, cannot be ruled out. If the ligand conformation in those species hinders the formation of Cu−N bonds, they will represent dead ends in the reaction mechanism, and consequently, their formation will result in a decrease in the overall rate of complex formation that will be more important as the number and stability of those outer-sphere complexes with geometries inadequate for complex formation increase. Thus, significant deviations from the estimations of the rate constants for the Eigen−Wilkins mechanism must be expected both for the simple approach using the Fuoss equation and for the more elaborate one including Rorabacher's steric factors. Those deviations will be different for each particular ligand, and they are expected to become more important as the structural complexity of the ligand increases.

Acknowledgment. Financial support from the Spanish MICINN (CTQ2006-15672-CO5-01, CTQ2006-14909-C02-01 and CTQ2009-14443-C02-01), Junta de Andalucía (Grupo FQM-137), and Generalitat Valenciana (GV06/258) is gratefully acknowledged. Ph.D. grants from MCYT (S.B.), MICINN (A.G.A.) and Universidad de Cádiz (C.E.C.) are also acknowledged.

Supporting Information Available: Figures with species distribution curves and NMR spectra, a list with the Cartesian coordinates of all the species calculated by using DFT procedures, more information regarding DFT caluclations, and a crystallographic information file. This material is available free of charge via the Internet at http://pubs.acs.org.